Pharmacological Research 175 (2022) 105982

Contents lists available at ScienceDirect

Pharmacological Research

journal homepage: www.elsevier.com/locate/yphrs

DNA aptamers masking angiotensin converting enzyme 2 as an innovative way to treat SARS-CoV-2 pandemic

Alessandro Villa [a,1], Electra Brunialti [a,1], Jessica Dellavedova [a], Clara Meda [a], Monica Rebecchi [a], Matteo Conti [d], Lorena Donnici [d], Raffaele De Francesco [d,e,1], Angelo Reggiani [b], Vincenzo Lionetti [c], Paolo Ciana [b,*]

[a] Department of Health Sciences, University of Milan, Milan 20146, Italy
[b] D3 Validation Research Line, Istituto Italiano di Tecnologia, Genoa 16163, Italy
[c] Institute of Life Sciences, Scuola Superiore Sant'Anna, Pisa 56127, Italy
[d] INGM - Istituto Nazionale Genetica Molecolare "Romeo ed Enrica Invernizzi", Milan 20122, Italy
[e] Department of Pharmacological and Biomolecular Sciences, University of Milan, Milan 20133, Italy

ARTICLE INFO

Keywords:
Coronavirus
SARS-CoV-2 variants
COVID-19 therapy
Nucleic acid-based drugs
ACE2

ABSTRACT

All the different coronavirus SARS-CoV-2 variants isolated so far share the same mechanism of infection mediated by the interaction of their spike (S) glycoprotein with specific residues on their cellular receptor: the angiotensin converting enzyme 2 (ACE2). Therefore, the steric hindrance on this cellular receptor created by a bulk macromolecule may represent an effective strategy for the prevention of the viral spreading and the onset of severe forms of Corona Virus disease 19 (COVID-19). Here, we applied a systematic evolution of ligands by exponential enrichment (SELEX) procedure to identify two single strand DNA molecules (aptamers) binding specifically to the region surrounding the K353, the key residue in human ACE2 interacting with the N501 amino acid of the SARS-CoV-2 S. 3D docking *in silico* experiments and biochemical assays demonstrated that these aptamers bind to this region, efficiently prevent the SARS-CoV-2 S/human ACE2 interaction and the viral infection in the nanomolar range, regardless of the viral variant, thus suggesting the possible clinical development of these aptamers as SARS-CoV-2 infection inhibitors. Our approach brings a significant innovation to the therapeutic paradigm of the SARS-CoV-2 pandemic by protecting the target cell instead of focusing on the virus; this is particularly attractive in light of the increasing number of viral mutants that may potentially escape the currently developed immune-mediated neutralization strategies.

1. Introduction

The severe acute respiratory syndrome coronavirus 2 (SARS-CoV-2) is an enveloped, non-segmented, positive sense RNA virus that causes COVID-19, a highly contagious zoonosis mostly transmitted through airborne droplets and characterized by a wide spectrum of damages on different vital organs including the lungs, heart, blood vessels, central nervous system and intestine [1], even if detection of infectious SARS-CoV-2 in the bloodstream remains controversial [2–4]. The COVID-19 case fatality rate in the worldwide population is 2.2% (https://ourworldindata.org/mortality-risk-covid?country=~OWID_WRL), although the likelihood increases with age and the presence of co-morbidities, reaching a value of 64% for elderly patients with 3 or more co-morbidities [5,6]. The molecular interaction between the receptor binding domain (RBD) of the activated S1 subunit of its S protein and the membrane bound ACE2 [7,8], which leads to rapid endocytic entry of the virus into the host cell [9] plays crucial role in the widespread diffusion of SARS-CoV-2. Within the specialized portion of

Abbreviations: aa, amino acids; ACE, angiotensin converting enzyme 2; Apt, aptamer; BR, Brazilian variant (P.1); BSA, buried surface area; COVID-19, Corona virus disease 19; ePCR, emulsion polymerase chain reaction; GMP, good manufacturing practice; RAAS, renin-angiotensin-aldosterone-system; RBD, receptor binding domain; S, spike; SA, South African variant (B.1.53); SARS-CoV-2, severe acute respiratory syndrome coronavirus 2; SELEX, systematic evolution of ligands by exponential enrichment; UK, United Kingdom variant (B.1.1.7); wt, wild-type Wuhan variant.

* Corresponding author.
E-mail address: paolo.ciana@unimi.it (P. Ciana).
[1] Equal contribution

https://doi.org/10.1016/j.phrs.2021.105982
Received 14 July 2021; Received in revised form 9 November 2021; Accepted 9 November 2021
Available online 16 November 2021

the ACE2 receptor, the K353 residue was shown to be important for the infectivity of several members of the *Orthocoronavirinae subfamily*, comprising SARS-CoV-1, SARS-CoV-2 and its variants, and HCoV-NL63 [10,11]. The recent observation that in *M. musculus,* the ACE2 K353H substitution protects the species from the SARS-CoV-2 infection further highlights the critical role played by this residue in the virus life cycle [12]. Since the beginning of the pandemic, several treatments have been proposed to limit worsening of symptoms due to cytokine storm and to prevent hospitalization, including the repurposing of existing drugs [13–16], natural products and herbal medicines [17] or a combination of both [18], some of which successfully reduced hospitalization or favored recovery from the disease [15,19]. Recently developed vaccines [20] and neutralizing monoclonal antibodies [21,22] have demonstrated particular efficacy in prevention and progression of severe COVID-19 [23,24], decreasing hospitalization and intensive care unit (ICU) admissions [25], although it is conceivable that the treatment tools targeting viral S1 might be less efficient in hampering the spread of different SARS-CoV-2 variants in the worldwide population [26] which displayed higher probability of infectivity [27] and mortality [28,29] than the original Wuhan strain [30]. To circumvent this plausible concern, new approaches blocking the entry of all SARS-CoV-2 variants into the host cells through the steric hindrance of human ACE2 K353 may represent an effective strategy for prevention of severe COVID-19 disease. For instance, this strategy was successfully applied in the case of the antiviral maraviroc, that binds to the C-C Motif Chemokine Receptor 5 and prevents the interaction of the human immunodeficiency virus type 1 with the target cell [31]. However, the timeframe needed for drug discovery and development of a small molecule hampering the interaction between SARS-CoV-2 and the ACE2 receptor might not be compatible with the current world-scale urgency. This time period is expected to be significantly shortened for other types of therapeutics including nucleic acids-based drugs such as aptamers, short single-stranded nucleic acids (RNA or DNA) that can specifically and efficiently bind to the target in the nanomolar range and disrupt protein/protein interactions [32,33]. Aptamers display great specificity and affinity, low immunogenicity and toxicity, an easy GMP-compliant method of production, and, especially noteworthy, a simple method of identification, all qualities that often make aptamers preferred candidates, also when compared for example with antibodies [33,34]. Indeed, the identification of aptamers with high affinity for a specific target, e.g. the ACE2 hotspot, relies on a well-established and efficient procedure: the systematic evolution of ligands by exponential enrichment, or SELEX [32]. SELEX is an *in vitro* selection procedure based on the iterative repetition of a target-driven PCR amplification cycle: this methodology, starting from a library of random single strand DNA or RNA oligonucleotides enriches the amplification products with pool of oligonucleotides with high affinity for the molecular target used for the selection. These oligonucleotides are univocally identified through next-generation sequencing of the nucleic acids present in the mixture. Here, we set up a specific SELEX procedure to isolate single strand DNA oligonucleotides that can selectively and efficiently recognize the ACE2 domain containing the K353 residue. Then, by applying *in vitro* and *in silico* approaches, we demonstrated that these aptamers could generate a steric hindrance on ACE2, thus preventing the binding of the cleaved S1 subunit SARS-CoV-2 S to the cellular receptor regardless of the viral variant and inhibiting the infection of pseudoviral particles carrying the S protein from SARS-CoV-2.

2. Methods

2.1. Oligopeptide selection

The consensus sequences of human ACE2 (accession number Q9BYF1) and mouse ACE2 (accession number Q8R0I0) were obtained from the UNIPROT database. Sequences spanning 25 aa and containing the 353 residues were designed and the tertiary structure was calculated using PEP-FOLD 3 [35] with preset data for 3D modeling. 3D structures were compared with the corresponding ACE2 structure using Chimera X 1.1 software (https://www.cgl.ucsf.edu/chimerax/) in order to find the peptides showing a three-dimensional structure most closely approaching that observed in the naïve protein.

2.2. SELEX procedure

The SELEX procedure was performed using XELEX DNA Core Kit (E3650, EURx). The human and mouse ACE2 oligopeptides (DPGNVQ KAVCHPTAWDLGKGDFRIL and EPADGRKVVCHPTAWDLGHGDFRIK) with a biotin tag at the N-terminal site were synthesized by Thermo Fisher Scientific and dissolved at a final concentration of 4 mg/ml in 50% DMSO water solution. For the oligopeptide-beads preparation, 80 μg of ACE2 oligopeptide (human or murine) was diluted in PBS pH 7.4 at the final concentration of 80 μg/ml and incubated with 2 mg of PBS-washed Dynabeads™ MyOne™ Streptavidin C1 (65001, Invitrogen) on a rotating shaker for 30 min followed by four washes with PBS pH 7.4. To block the remaining free streptavidin sites, the reaction was incubated with 1 μM biotin for 5 min, followed by 4 washes and resuspended in the SELEX buffer (NaCl 140 mM, KCl_2 mM, $MgCl_2$ 5 mM, $CaCl_2$ 2 mM, Tris pH 7.4 20 mM, Tween 20 0.05% [v/v]). The ACE2-beads were immediately used for the SELEX procedure.

Each oligo in the ssDNA library contained a core randomized sequence of 40 nucleotides (nt) flanked on both sides by two sequences of an 18-base pair, identical in all oligos, needed for primer hybridization during the PCR amplification step (5'-TGACACCGTACCTGCTCT-40nt randomized sequence -AAGCACGCCAGGGACTAT-3'). For the first round of selection, 4 nmol of the ssDNA library were resuspended in 500 μl SELEX buffer and incubated with 2 mg of ACE2-coated beads at 37 °C on a rotating shaker for 60 min; afterward, the beads were washed with 0.3 ml Selex buffer at 37 °C and bound aptamers were immediately eluted through denaturation at 92 °C for 3 min in distilled water; half of the solution was used to perform an emulsion PCR (ePCR), a technique used to enrich the number of copies of individual sequences in the amplification reaction. The amplified DNA was purified with DNA Spin Column, diluted in Selex buffer, heated at 94 °C for 3 min and cooled immediately on ice for 5 min; the same denaturation-renaturation procedure was performed before each binding step with ACE2-coated beads. For the negative selection, 50 pmol of the first cycle of positive selection were incubated with 0.2 mg of beads (without peptide) for 30 min at 37 °C; afterwards, the non-bound DNA in the supernatant was collected and incubated with 1 mg of beads coated with human or mouse ACE2. In order to pick up aptamers with high affinity and specificity, the positive selection cycle (elution, ePCR, purification, denaturation and renaturation steps) was repeated 10 times, moreover, the DNA-bead incubation time was gradually decreased (from 60 to 30 min) and the wash strength was enhanced by increasing the volume (from 300 to 700 μl) and the number of washes (from 1 to 2 times). The polymerase chain reactions for the amplification of the sequences were performed in emulsion (ePCR) (E2500, Eurx). The PCR mixtures in Pol buffer A contained, 1.5 mM MgCl2, 0.01 mg/ml acetylated bovine serum albumin, 400 nM each primer, 0.4 mM each dNTP, and 2 U EURx DNA polymerase in a total volume of 50 μl. 300 μl of prechilled oil surfactant mixture were vortexed with 50 μl PCR mix for 5 min, dispensed into PCR tubes; the PCR thermal cycle conditions were: 95 °C for 2 min followed by 20 cycles of 95 °C for 30 s, 55 °C for 60 s, 72 °C for 3 min; the final extension was carried out at 72 °C for 5 min. When sufficient amplified material was recovered from the PCR reaction, the DNA was subjected to Next Generation Sequencing (Illumina MiSeq).

2.3. Single cycle SELEX assay

The binding ability of each aptamer to the human ACE2 peptide was evaluated with a single cycle SELEX assay. To this end, each synthesized aptamer (Sigma) was diluted in SELEX buffer at the final concentration

of 0.2 μM, subjected to the denaturation-renaturation procedure (see "SELEX procedure" paragraph) in a final volume of 250 μl; 0.1 mg beads coated with the human ACE2 oligopeptide or, in another reaction the same amount of uncoated beads, were added to the denatured-renatured aptamers and then incubated for 1 h at 37 °C with gentle agitation; after incubation, beads were washed twice with 1 ml SELEX buffer at 37 °C and the DNA was finally eluted from the beads through denaturation at 92 °C for 3 min in 200 μl of nuclease free water; 5 μl of the solution was assayed in a qRT-PCR reaction in triplicate using SYBR green and GoTaq qPCR Master Mix (A6001, Promega) according to the manufacturer's protocol. The reaction was carried out in a QuantStudio™ 3 Real-Time PCR system (ThermoFisher scientific) programmed with the following thermal profile: 2 min at 95 °C, then 40 cycles of 15 s at 95 °C, 1 min at 60 °C using the same primers used for the ePCR.

2.4. ELISA assay to test the inhibition of the RBD SARS-CoV-2 S/ACE2 interaction

The ability of aptamers to interfere with the RBD SARS-CoV-2 S/ACE2 interaction was assayed with the SARS-CoV-2 (COVID-19) Inhibitor Screening Kit from Acrobiosystems (EP-105) following the manufacture's protocol. Briefly, S proteins (wt: Cat # A010–214, Acrobiosystems; B.1.351: Cat # S1N-C52Hm, Acrobiosystems) diluted in Coating Buffer to a final concentration of 0.3 μg/ml were added to 96-well plates and incubated overnight (~16 h) at 4 °C. The uncoated proteins were removed by washing the wells three times with a washing buffer (PBS with 0.05% Tween-20, pH 7.4) and blocked for 1 h at 37 °C in blocking buffer (PBS with 0.05% Tween-20% and 2% bovine serum albumin, pH 7.4). The interference of the aptamer with the RBD SARS-CoV-2 S/ACE2 interaction was determined by incubating increasing concentrations of aptamer with the biotinylated human ACE2 provided in the kit, for 1 h at 37 °C in the incubation buffer (EP-105, Acrobiosystems), and then added to the S-coated wells and incubated for 1 h at 37 °C. At the end of the incubation time, the wells were washed three times with Wash Buffer and incubated for 1 h with 100 μl of HRP-conjugated streptavidin (1:5000) (EP-105, Acrobiosystems); after three washes with washing buffer, the 3,3',5,5'-Tetramethylbenzidine (TMB) substrate (CL07, Merck) of HRP was added to the reaction following the manufacturer's instruction, finally, the reaction was stopped with 1 M sulfuric acid (100 μl/well) (Q29307, Thermofisher). The binding of the biotinylated ACE2 with the RBD SARS-CoV-2 S in the coated wells was measured as absorbance value at 450 nm wavelength using a microplate reader (Biorad).

2.5. Generation of HEK293TN cells overexpressing the human ACE2 protein

HEK293TN cells (obtained from System Bioscience) were engineered by lentiviral transduction to stably express human ACE2 receptor (HEK293TN-hACE2). Lentiviral vectors were produced following a standard procedure based on calcium phosphate cotransfection with 3rd generation helper and transfer plasmids. The following helper plasmids were gifts of Didier Trono: pMD2. G/VSV-G (Addgene #12259), pRSV-Rev (Addgene #12253), pMDLg/pRRE (Addgene #12251). The transfer vector pLENTI_hACE2_HygR was obtained by cloning of human ACE2 from pcDNA3.1-hACE2 (a gift from Fang Li, Addgene #145033) into pLenti-CMV-GFP-Hygro (a gift from Eric Campeau & Paul Kaufman, Addgene #17446). Human ACE2 was amplified by PCR and inserted under the CMV promoter of the pLenti-CMV-GFP-Hygro after GFP excision with *Xba*I and *Sal*I digestion. The human ACE2 lentiviral vector thus obtained was used to transduce HEK293TN. 48 h after transduction, cells were subjected to antibiotic selection (250 μg/ml hygromycin). Expression of human ACE2 in transduced cells was confirmed by flow cytometry and immunofluorescence (see below) and found to be stable after several cell passages. HEK293TN-hACE2 cells were maintained in DMEM, supplemented with 10% FBS, 1% glutamine, 1% penicillin/streptomycin and 250 μg/ml Hygromycin (GIBCO).

2.6. Plasmid generation and transient transfections

The plasmids for the transient transfection were purchased from Vector Builder; in brief they were generated by cloning the open reading frame from hACE2 or mAce2 downstream the CMV promoter into the mammalian expression vector pRP[Exp]-CMV. The A549 cell line was purchased from the American Type Culture Collection ATCC and grown in DMEM (32430–027, Thermo Fisher Scientific), supplemented with 10% FBS (ECS0186L, Euroclone), 1% GlutaMAX (35050–061, Thermo Fisher Scientific), 1% penicillin/streptomycin (15240–062, Thermo Fisher Scientific) in a humidified 5% CO_2-95% air atmosphere at 37 °C. For the transfection 30,000 cells/well were seeded in chambered coverglass (155411, Thermo Fisher Scientific) and cultured overnight prior to transfection. The transfections were carried out using Lipofectamine 3000 (L3000001, Thermo Fisher Scientific) following the manufacturer's instructions with 210 ng DNA, 0,6 μl lipofectamine 3000, and 0,4 μl P3000 reagent for each well; 40 h after transfection the cells were stained with Apt.6 conjugated with Alexa 546.

and subject to confocal live imaging, and then fixed for ACE2 immunostaining.

2.7. Confocal Imaging of live cells stained with the aptamers conjugated with Alexa 546

Fluorescence images of HEK293TN, HEK293TN-hACE2, and A549 transient transfected cells bound with the aptamer conjugated with Alexa 546 (synthesized by Integrated DNA Technologies, Inc.) were acquired by laser confocal fluorescence microscopy (ZEISS LSM 900). 10 μg/ml DAPI was added to HEK293TN-ACE2 bound with the Alexa 546 Apt. 6 or scrambled and acquired with an Axiovert 200 M microscope. Cells were pre-incubated with 4 mM mock DNA oligo (20 bp) for 5 min on ice and then with 100 nM Alexa-labelled aptamer on ice for 7 min in the dark. The supernatant was removed, and cells were washed once with Selex buffer and twice with ice-cold HBSS (14175095, Thermo Fischer Scientific) prior to confocal imaging.

2.8. Immunostaining of the human ACE2

HEK293TN, HEK293TN-hACE2, and A549 transient transfected cells grown on chambered coverglass (155411, Thermo Fisher Scientific) were fixed with 4% paraformaldehyde for 15 min and washed with PBS, then incubated for 90 min in PBS with 10% normal goat serum at RT (G9023, Merk). Subsequently, they were incubated with human ACE2 antibody (1:50) (ab108252, Abcam) in 1% normal goat serum, overnight at 4 °C. After four washes with PBS, cells were incubated with the secondary antibody AlexaFluor anti-Rabbit 488 (1:200 in PBS) (A32731, Thermo Fisher Scientific) for 1 h at room temperature, then stained with DAPI (1:1000) (D1306, Thermo Fisher Scientific) to label cell nuclei prior to confocal imaging (ZEISS LSM 900).

2.9. FACS analysis for detection of surface expression of human ACE2 in HEK293TN and HEK293TN-hACE2 cell lines

Live cell staining was performed by incubation of HEK293TN or HEK-293 T-hACE2 cells with Anti-hACE2 antibody (AF933, R&D systems) at 0.75 μg/200.000 cells for 1 h at 37 °C. This was followed by incubation with anti-goat Alexa Fluor 647TM secondary antibody (1:200 in PBS + 2% FBS) for 30 min at 37 °C. Goat IgG Isotype was used as negative control. Data were acquired on a BD FACS Canto II and analyses were performed using FlowJo software.

2.10. Production of lentiviral-based SARS-CoV-2 pseudoparticles

Lentiviral SARS-CoV-2 pseudotype particles encoding for luciferase

reporter gene were produced as described in [36]. Briefly, HEK293TN cells were co-transfected with reporter plasmid pLenti CMV-GFP-TAV2A-LUC Hygro, pMDLg/pRRE (Addgene #12251), pRSV-Rev (Addgene #12253) and pcDNA3.1_Spike_del19 (Addgene #155297). To obtain the viral pseudoparticles, the supernatant was collected 30 h after transfection, clarified by filtration and concentrated by ultracentrifugation for 2 h at 20,000 rpm.

2.11. Luciferase based pseudoviral entry assay

HuH 7.5 cells were seeded in 96-well plates in 100 ml medium at 10,000 cells/well. The next day, the media was replaced with physiological buffer (NaCl 140 mM, KCl_2 mM, $MgCl_2$ 5 mM, $CaCl_2$ 2 mM, Tris pH 7.4 20 mM) and cells were incubated for 10 min at 37 °C with increasing concentrations of Apt.6 for 10 min. Subsequently, SARS-CoV-2 pseudoparticles were added at 1 MOI and cells were incubated for 7 min at 37 °C. After incubation, cells were washed with PBS to remove unbound pseudoparticles, and maintained at 37 °C in complete medium. After 48 h, cell infection was measured by luciferase assay, using Bright-Glo™ Luciferase System (Promega), and Infinite F200 plate reader (Tecan) was used to read luminescence, expressed as relative light units (RLU).

2.12. Computational methods

The consensus sequence of human ACE2 was obtained from the UNIPROT database (accession number Q9BYF1). Homology studies were performed using the Basic Local Alignment Search Tool (BLAST) for regions of local similarity between the consensus sequences of ACE2 in selected mammalians: Macaca mulatta, sequence ID: EHH30556.1; Bos taurus, sequence ID: NP_001019673.2; Sus scrofa, sequence ID: NP_001116542.1; Rattus norvegicus, sequence ID: NP_001012006.1; Mus musculus, sequence ID: ACT66269.1. The secondary structures of aptamers were calculated using the UNAFOLD web server [37], while tertiary structures were calculated, starting from the secondary structures, using the 3D-DART software [38].

For the docking experiments, the co-crystallized structure of human ACE2 receptor with S protein (PDB id: 6VW1) was separated into its receptor (ACE2) and ligand (S) components, which were used as starting models. The structures of mutant SARS-CoV-2 S proteins were derived from https://spikemutants.exscalate4cov.eu/. To identify the most stable complexes (poses) of human ACE2 with SARS-CoV-2 S protein and with the aptamers, the docking program HADDOCK (version 2.4) was used with standard parameters. HADDOCK uses an initial rigid-body docking process, which generates typically a large number of poses, in the order of thousands. From these, several hundred were selected for further flexible refinement and scoring using HADDOCK score, Van-der-Waals and electrostatic interactions to identify the best docking pose.

3. Results

3.1. Identification of a minimal polypeptide in the human ACE2 protein for the SELEX procedure

Among the 10^{15} molecules present in the single strand DNA bank, we have chosen the correct bait for the SELEX procedure to select the aptamers appropriately interacting and sterically cluttering the region surrounding the K353 residue of the human ACE2 [39]. To this aim, we initially characterized the 3D structure of the domain responsible for the interaction between human ACE2 and viral S glycoprotein to design the minimal oligopeptide, able to correctly reproduce the 3D structure surrounding K353, e.g., containing the entire loop with the two anti-parallel beta-sheets (Fig. 1A). This bioinformatic analysis identified the 25-amino acid peptide DPGNVQKAVCHPTAWDLGKGDFRIL as the minimal sequence correctly modelling the 3D loop structure comprising the K353 residue in the native protein. The oligopeptide included a core sequence conserved across different mammalian species and a more variable NH2 terminal (Fig. 1C and S1) mapping right before the first beta sheet.

We extended the analysis of the 3D structure on the murine ACE2 to verify whether the presence of a histidine in position 353, that confers protection form SARS-CoV-2 infection, would have changed the shape of the S interacting domain. We showed that the K353H amino acid substitution in the corresponding mouse peptide, EPADGRKVVCHPTAWDLGHGDFRIK, did not produce any spatial distortion of the structure immediately surrounding the residue. On the contrary, the divergent amino acid sequence in the N-terminal part of the peptide generated a different 3D structure between the two species (Fig. 1B). Hence, we hypothesized that an aptamer interacting with the common core of the mouse and human ACE2 sequences would have been able to bind that region independently from the amino acid present at position 353, an important feature since this amino acid is polymorphic in humans [40]. This observation prompted us to apply both human and mouse oligopeptides to the SELEX protocol for the identification of molecules binding to this common core sequence.

3.2. Aptamer identification through the SELEX procedure

The SELEX procedure was carried out according to a standard protocol [32]. The first SELEX cycle was done with the human ACE2 peptide followed by a negative selection with uncoated beads to remove nonspecific binding molecules; afterward, the reaction mix was split in two parallel selections driven by the human and mouse peptides (Fig. 2A and S2).

Next generation sequencing (NGS) was applied to each cycle, when sufficient amplified material was recovered (Fig. 2A); sequences significantly represented over background levels, appeared only after the 4th cycle and we decided to consider only those representing more than 0.1% of the total (Table S1). Eight unique sequences were identified together with three variants of the sequence no. 1 differing by a single point mutation (collectively indicated as sequence no. 9 *). Sequences no. 1–3 were found in both selections with human and mouse ACE2 oligopeptide, no. 4–7, 9 were specific for the human ACE2 oligopeptide and no. 8 was found to be highly specific for the mouse ACE2 selection, although it was represented also in the human selection, to a lesser extent. Sequence no. 6 was incomplete and was excluded from further experiments.

Since PCR amplification resulting from the SELEX cycle produced dsDNA, it is not possible to predict which of the two strands is the peptide-interacting ssDNA; thus, we chemically synthesized the fourteen possible aptamers out of the seven sequences isolated with the SELEX procedure (Table S2).

Aptamers were then tested for their specific binding ability on the human ACE2 peptide with a single cycle SELEX assay carried out with each pure aptamer as unique source of ssDNA and with beads coated with the human ACE2 peptide or uncoated (Fig. S3). The results of these experiments identified, for each sequence, the DNA strand that established a productive interaction with the human ACE2: aptamers (Apt.) no. 1, 4, 6, 9, 12, 14 were highly enriched compared to their corresponding strand, while neither of the two strands of sequence 4 (Apt. 7 and 8) showed a significantly higher affinity for the peptide coated beads in this binding assay (Fig. 2B).

3.3. Aptamers hinder the SARS-CoV-2 S/ACE2 interaction

Next, we tested the ability of the selected aptamers to interfere with the SARS-CoV-2 S /human ACE2 interaction; to this purpose we used an ELISA assay based on the interaction of the SARS-CoV-2 S RBD, immobilized on a multiwell plate, with a biotinylated human ACE2 recombinant protein. The binding of ACE2 was measured with a colorimetric assay based on the substrate oxidation that follows the HRP-conjugated streptavidin/biotin interaction. The binding reaction was carried out in

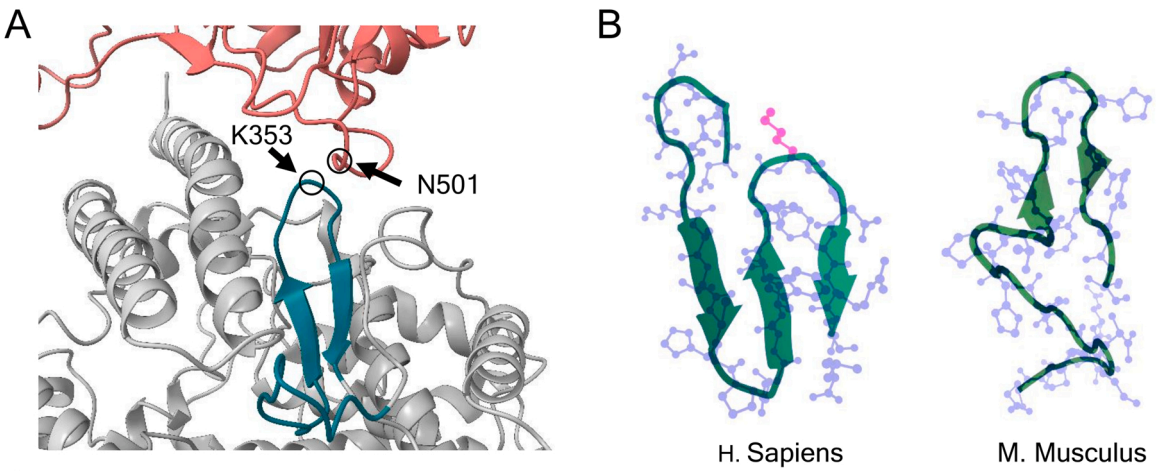

Fig. 1. Selection of the oligopeptide for the SELEX procedure of aptamer identification. (A) Representative scheme of a detail of SARS-CoV-2 RBD (pink) and human ACE2 complex, modelled using the high ambiguity driven protein-protein docking software (HADDOCK) v. 2.4, showing the interaction between RBD-N501 residue and ACE2-K353. The portion of ACE2 highlighted in green represents the sequence selected for the synthesis of the human ACE2 peptide, used as a bait for the SELEX procedure. (B) Representation of the tertiary structures of the human and murine ACE2 peptides, *de novo* calculated using PEP-FOLD-342. (C) Sequence comparison of the human ACE2 consensus (aa 301–400) including the ACE2-K353 residue with the same consensus in different mammals that are potentially affected (*Macaca mulatta, Bos taurus Sus scrofa*), and unaffected (*Rattus norvegicus, Mus musculus*) by SARS-CoV-2. The red text and the box show the sequence selected for the generation of human and murine ACE2 synthetic peptides. aa: amino acids; Norv: norvegicus; RBD: receptor binding domain.

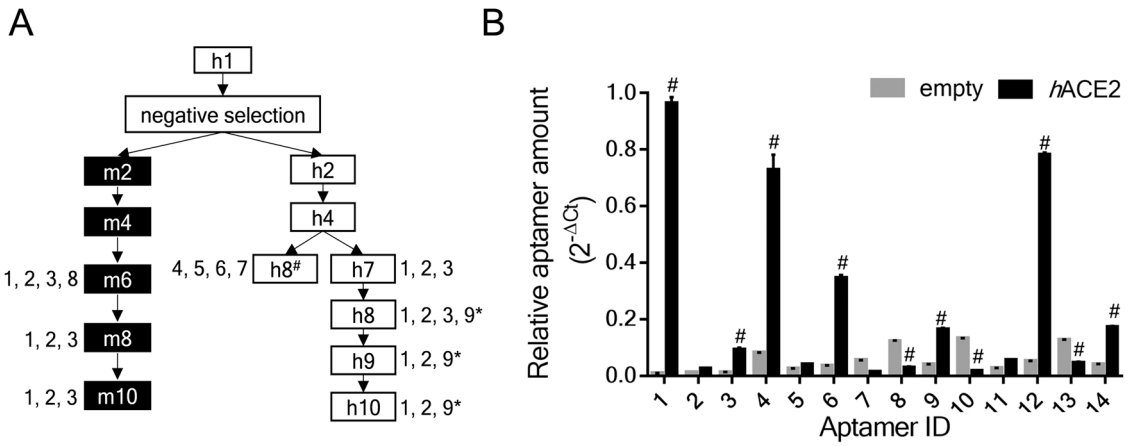

Fig. 2. Identification of aptamers with high affinity for the human ACE2 peptide. (A) Scheme of the aptamer selection through the human and mouse ACE2 oligopeptide. The cycle number for each selection, as well as the enriched sequences identified by NGS are given. Only enriched sequences representing more than 0.1% of the total were considered. SEQ 1, 2, 3 were present in both human and mouse selections. (B) Evaluation of the specific human ACE2 binding ability for each aptamer. The recovery from a single SELEX cycle carried out with each purified aptamer was measured by qRT-PCR. Bars in the graph show the relative aptamer amount eluted from the empty beads (light grey) or the beads coated with human ACE2 peptide (black) quantified with the method of the $2^{-\Delta Ct}$ versus the highest threshold cycle (Ct). Data are mean values ± SD of 3 technical replicates, #P < 0.0002 calculated with 2-way ANOVA followed by Sidak's multiple comparisons test vs empty beads. h: human; m: mouse.

the presence of high (1 μM) and low (10 nM) concentrations of each aptamer. Only Apt. 6 and 14 significantly reduced more than 50% the SARS-CoV-2 S/ACE2 interaction, (Fig. 3A); conversely, Apt. 1 just halved the percentage of binding in a dose-independent manner even if it showed the best specific/nonspecific ratio in the human ACE2 coated beads-binding assay (Fig. 2B).

A wider range of concentrations from (10 nM) to (1 μM) was then tested in the same ELISA assay for Apt. 6, Apt. 14 and Apt. 1 to measure the IC50 of the SARS-CoV-2 S/human ACE2 binding inhibition. Apt. 6 showed the lowest IC50 (35 nM) in the range of concentration of the positive control provided by the manufacturer of the kit, Apt. 14 had a higher IC50 of 132 nM, while it was confirmed that Apt. 1 lacked any inhibitory activity (Fig. 3B). Next, we also tested the aptamer binding ability to the ACE2 receptor on *in vitro* cell culture. To this end,

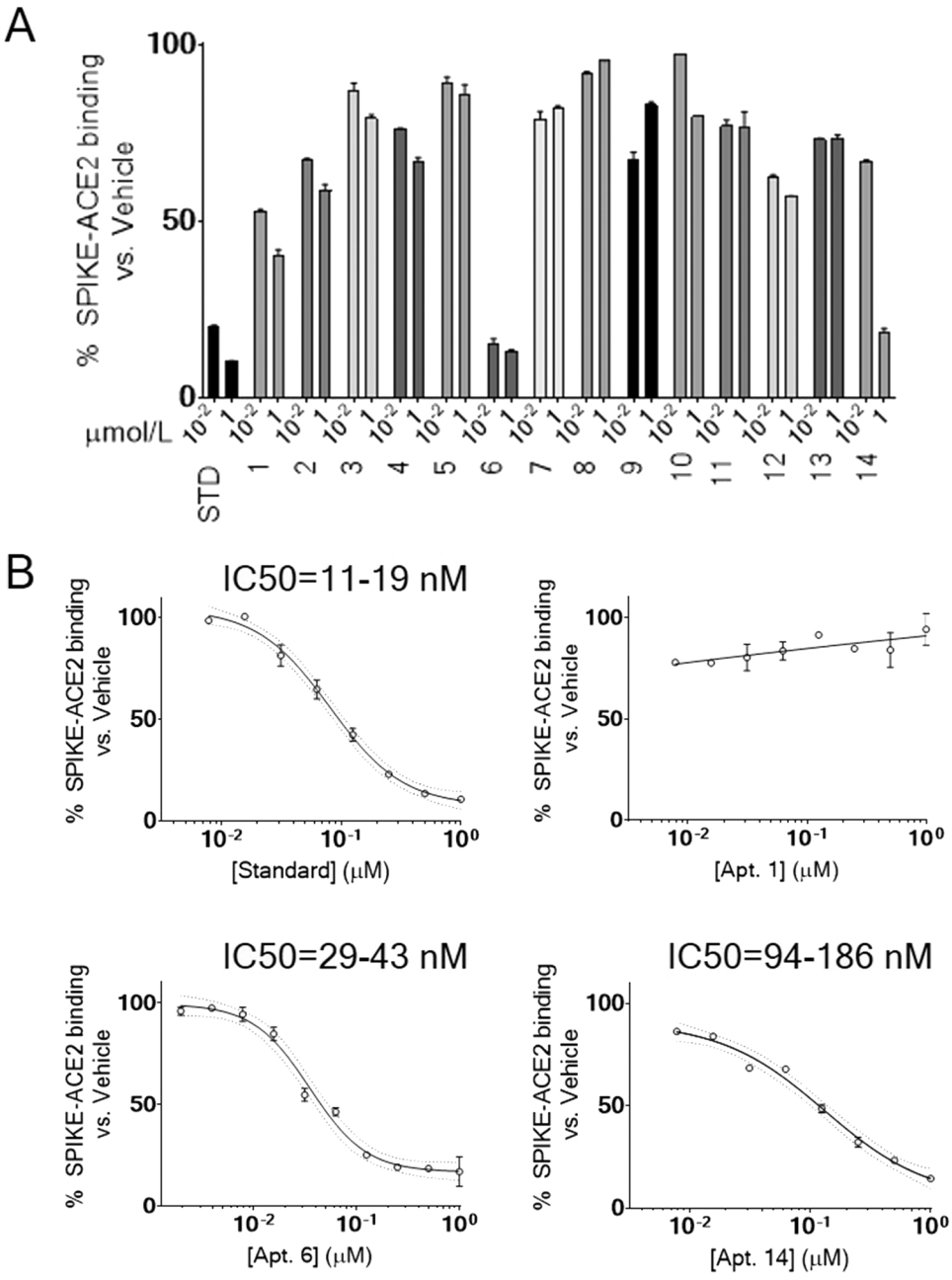

Fig. 3. Inhibition of the human ACE2/SARS-CoV-2 S protein RBD interaction by selected aptamers. (A) Binding of SARS-CoV-2 S protein RBD coated on a 96-well ELISA plate with a biotinylated human ACE2, pre-incubated for 1 h with either the reference inhibitor or the aptamers identified with the SELEX procedure (Apt. numbers 1–14) at 2 different concentrations (10 nM and 1 µM). Binding is expressed as a percentage versus vehicle-incubated biotinylated human ACE2, as determined by a colorimetric assay at 450 nm wavelength. (B) IC50 determination for Apt. 1, 6, and 14 with the same assay as in (A). Binding is expressed as percentage versus vehicle-incubated biotinylated human ACE2, as determined by a colorimetric assay at 450 nm wavelength. Dotted lines indicate 95% C.I. profile. Apt.: aptamer; STD: standard.

HEK293TN cells transduced with a lentiviral vector expressing the human ACE2 receptor or the parental cell line (Fig. S4) were incubated with an Alexa-fluor modified Apt.6. The results clearly demonstrate the fluorescent signal, specific for the membrane-bound ACE2 in transfected cells (Fig. 4A), confirming that the binding ability occurs also with the ACE2 receptor when located in the cell membrane. The membrane staining due to Alexa-fluor modified Apt. 6 was also detected when A549 adenocarcinomic human alveolar basal epithelial cells were transiently transfected with plasmids constitutively expressing human ACE2 or murine ACE2, a pattern not detected when the cells were transfected with the empty vector or when HEK293TN-ACE2 were stained with a scrambled aptamer (Fig. 4B, S5 and S6).

Finally, we tested the hypothesis that the aptamer binding to the ACE2 receptor could led to the prevention of viral entry into the target cell. To this purpose, we have used a SARS-CoV-2 spike pseudotyped virus containing a luciferase reporter [36] to infect Huh7.5 cells, that physiologically express human ACE2 receptor on their cell membrane and can be efficiently infected by the lentiviral pseudotyped spike particles. The infection was carried out in the presence of increasing concentrations of Apt. 6. An anti hACE2 antibody (R&D Systems, AF933) at 20 µg/ml concentration was used as positive control for neutralization of infection. Luciferase activity in the cell extract provided a quantitative measure of the magnitude of infection (Fig. 4C). The results showed that Apt. 6 was able to inhibit the infection with a similar efficacy (−70%) of the neutralizing antibody and a potency in the range of the IC50 measured with the SARS-CoV-2 S/human ACE2 binding inhibition assay (Fig. 3B).

Altogether, these results indicated that the SELEX procedure successfully identified two aptamers binding with high affinity to the human ACE2, preventing its interaction with the SARS-CoV-2 S, thus inhibiting the viral entry into the target cell.

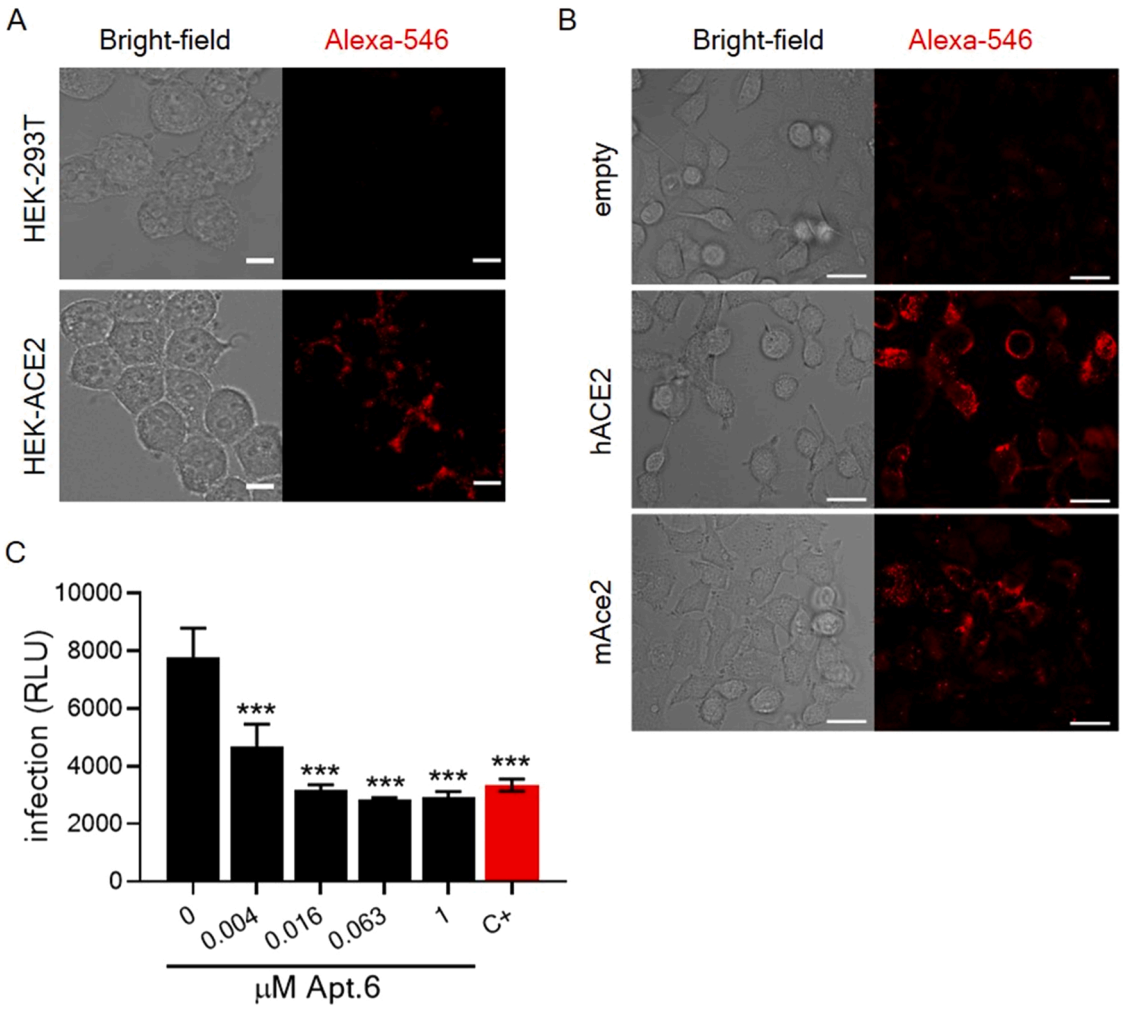

Fig. 4. Apt. 6 binds to the membrane ACE2 receptor and inhibits the viral entry into the target cell. (A) Confocal images of live HEK293TN and HEK293TN-ACE2 cells stained with the Alexa 546-labeled Apt.6. Left panel: bright field images; right panel: Alexa 546 fluorescence emitted from of 2.25 μm depth. Scale bar of 10 μm. (B) Confocal images of A549 cells transiently transfected with a vector constitutively expressing hACE or mAce2 or empty and live stained with the Apt. 6 conjugated with Alexa 546. Left panel: bright field images; right panel: Alexa 546 fluorescence emitted from of 4.0 μm depth. Scale bar of 25 μm. (C) The pseudoviral infection was quantified as the amount of luciferase expressed by the infected target cells. The graph reports the luciferase activity in the cell extract obtained after the infection carried out in the presence of increasing concentrations of Apt. 6 or 20 μg/ml of the neutralizing antibody anti-hACE2 used as positive control (C+). Bars show the mean value of the relative light units (RLU) ± SEM of triplicates. * **$p < 0.001$ versus vehicle calculated by one-way ANOVA followed by Dunnett's multiple comparisons test. Apt.: aptamer; HEK: HEK293TN; HEK-ACE2: HEK293TN-ACE2 S: spike; STD: standard reference inhibitor.

3.4. Molecular modelling of the aptamer-bound ACE2 receptor

To identify possible common features between the two aptamers hindering the SARS-CoV-2 S/ACE2 binding, we modelled their 2D and 3D structures using UNAFOLD [37] (for the secondary structure) and 3D_DART [38] (for the tertiary structure). Both secondary and tertiary folding did not show any common structures in the two aptamers: the intramolecular double strand formation was more pronounced in Apt. 14 (with respect to Apt. 6) likely conferring a more rigid structure when compared to Apt. 6 (Fig. S7) and no obvious common shape could be deduced from the 3D structures (Fig. S8).

To gain insight into the molecular mechanism of the aptamer-driven inhibition of the SARS-CoV-2 S/ACE2 binding, we modelled in silico the docking of the aptamer on human ACE2. For this purpose, the co-crystallized structure of the human ACE-2 receptor with the SARS-CoV-2 S (PDB id: 6VW1) was separated into its receptor (ACE2) and ligand (S) components. The receptor and ligand were then re-docked using HADDOCK v. 2.4 [41] with default settings to validate the docking procedure. The structure of human ACE2 was then used to determine the most stable docking poses of the complexes of the protein with the aptamers (Fig. 5). It was clear that both Apt. 6 and Apt. 14 masked the K353 residue of the human ACE2 receptor, while Apt. 1 interacted with another portion of the oligopeptide used for the SELEX (marked in blue in the figure) far away from the S interaction. These results provided the molecular explanation for the apparent discrepancy between the ability of Apt. 1 to interact with the peptide (Fig. 2B) and its null efficacy in the disruption of the SARS-CoV-2 S/human ACE2 interaction (Fig. 3B).

An in-depth inspection of Apt. 14 and Apt. 6 binding to the human ACE2 showed that Apt. 14 had the lowest values for Van der Waals and electrostatic interactions and the overall interacting surface (Buried Surface Area, BSA) was greater in Apt. 6 (Table 1). These data are in keeping with the lower IC50 for Apt. 6 and its greater ability to mask the K353 and prevent the SARS-CoV-2 S/human ACE2 interaction as experimentally demonstrated with the ELISA assay (Fig. 3B).

Further analysis of the base pairs of Apt. 6 and 14, interacting with the region surrounding the K353 revealed a common consensus present in the two aptamers (GA-C) establishing a stereo specific interaction in close proximity of the K353 task (Fig. S9). Exchanging the K353 residue with the H353, a polymorphism present in the human population, did not significantly change the binding ability of the two aptamers (Table S3).

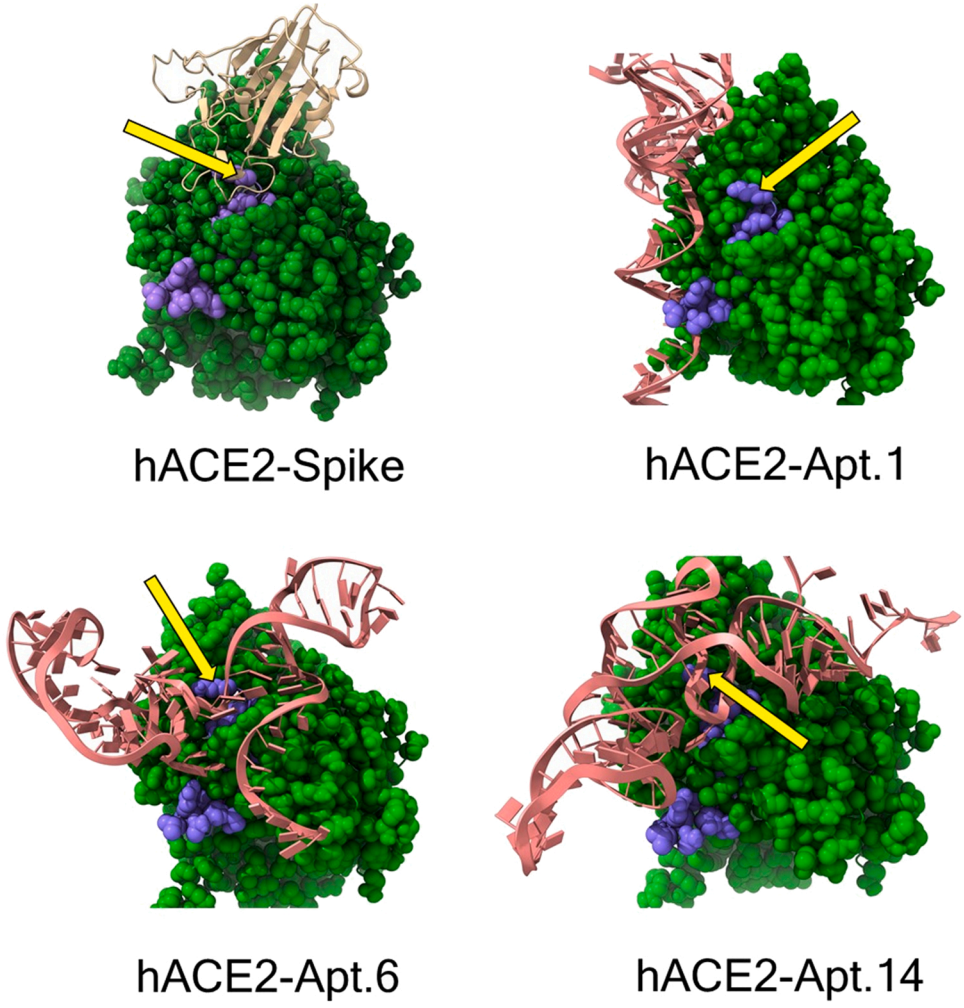

Fig. 5. Docking simulations of the identified aptamers. The pictures show the most stable configuration of the interaction between human ACE2 (green) with SARS-CoV-2 S protein (papaya yellow ribbon, upper left panel), Apt. 1 (pink tube/slab, upper right panel), Apt. 6 (pink tube/slab, lower left panel), and Apt. 14 (pink tube/slab, lower right panel). The amino acid sequence representing the peptide used as bait for the SELEX procedure is shown in blue. The yellow arrows indicate the position of the 353 hotspot. Apt.: aptamer. (For interpretation of the references to colour in this figure legend, the reader is referred to the web version of this article).

Table 1
Energetic calculations obtained with HADDOCK v. 2.4.

	Apt 6	Apt 14	Apt1	Apt5	Spike
Van der Waals (a.u.)	-111.5 ± 1.6	-65.8 ± 7.8	-88 ± 8.6	-15 ± 7.0	-59 ± 2.4
Electrostatic (a.u.)	-288.7 ± 41.8	-182.6 ± 9.0	-368.4 ± 38.1	-132.4 ± 15.8	-185.4 ± 8.7
BSA (Å^2)	3130.4 ± 394.9	2341.9 ± 138.0	2849.1 ± 165.5	604 ± 159.8	1729 ± 34.6

Van der Waals – van der Waals interaction score; Electrostatic – electrostatic interaction score; BSA – buried surface area; a.u. – arbitrary units of energy. Data are presented as mean values ± s.d.

The ability of different aptamers to block the SARS-CoV-2 S/human ACE2 interaction was tested *in silico*: when bound to the viral receptor, Apt. 6 or Apt. 14 were able to significantly hinder the interaction with the SARS-CoV-2 S of the Wuhan variant. Most importantly, the interaction of SARS-CoV-2 S with the UK, Brazilian and South African variants with human ACE2 were also hindered (Table 2), thus suggesting that selected aptamers are able to mask the interaction of any SARS-CoV-2 variants in the presence of any residue in position K353 in the human ACE2. To confirm the versatility of our aptamers to prevent interaction between the human ACE2 with the mutated S found in different human SARS-CoV-2 variants, a commercially available mutated S (L18F/ D80A/ D215G/ R246I/ K417N/ E484K/ N501Y/ D614G) identified in the SARS-CoV-2 variant (known as 20 C/501Y.V2 or B.1.351 lineage) circulating in South Africa was tested in the ELISA interference assay. The results revealed that both aptamers were able to

Table 2
Energetic calculations obtained with HADDOCK v. 2.4.

Variant	Binding affinity (ΔG, Kcal/mol)			Dissociation constant, (K_D, M)		
	No apt	Apt 6	Apt 14	No apt	Apt 6	Apt 14
wt	-10.7	-7.0	-8.7	3.8E-8	1.2E-5	7.9E-6
UK	-11.5	-8.7	-7.7	7.5E-9	7.3E-7	3.8E-6
SA	-13.7	-9.3	-8.2	2.1E-10	2.6E-7	1.8E-6
BR	-13.2	-6.2	-8.5	4.9E-10	6.9E-6	1.1E-6

wt: Wuhan variant, UK: United Kingdom variant (B.1.1.7), SA: South African variant (B.1.53), BR: Brazilian variant (P.1).

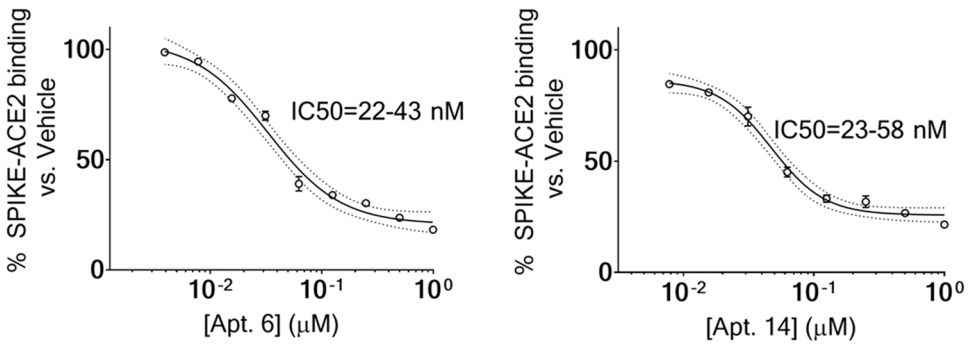

Fig. 6. Inhibition of the human ACE2/SARS-CoV-2 (B.1.351 lineage) S protein RBD interaction by selected aptamers. IC50 determination for Apt. 6 and 14, obtained by evaluating the binding of SARS-CoV-2 (B.1.351 lineage) S protein RBD coated on a 96-well ELISA plate with a biotinylated human ACE2 pre-incubated for 1 h with Apt. 6 or Apt. 14. Binding is expressed as percentage versus vehicle-incubated biotinylated human ACE2, as determined by a colorimetric assay at 450 nm wavelength. Dotted lines indicate 95% C.I. profile.

interfere with the binding of the mutated S to the human ACE2 in the nanomolar concentration range (Apt. 6 = 33 nm; Apt. 14 = 47 nm), thus validating the in silico prediction (Fig. 6).

4. Discussion

In this work, we present the initial experimental evidence that specific DNA aptamers binding the human ACE2 hinder its interaction with the SARS-CoV-2 S glycoprotein. Therefore, there is reason to be optimistic that the discovery of new human ACE2-targeted aptamers will help in managing SARS-CoV-2 infection by protecting target cells rather than increasing humoral immunity recognition, neutralization and subsequent elimination of the virus from the body (i.e. the mechanism of action of current therapies including vaccines, neutralizing monoclonal antibodies and small molecules, in preclinical or clinical development) [42–44]. To put in place our conceptually opposite paradigm, we have synthesized two specific DNA aptamers effectively binding the protein domain surrounding the human ACE2-K353, the residue of the receptor that plays a key role in the process leading to the SARS-CoV-2 entry into the host cell. The first obvious plus of our innovative approach is that the complex aptamer-human ACE2-K353 may prevent the SARS-CoV-2 infection, either of the wild type or its mutated variants. Moreover, our aptamers can be theoretically effective also against past and future coronavirus infections since the mechanism of interaction between the RBD of the activated viral S and human ACE2 is quite well conserved among different species of the *Orthocoronavirinae* subfamily [45].

Mutations randomly arising in the viral population may modify the antibody or drug target sites, thus escaping from their neutralization activity; we cannot ignore that the SARS-CoV-2 has already proved to have a mutation rate sufficiently high to create new variants, jeopardizing the effectiveness of the containment measures so far adopted [46], hence creating the condition for the spread of novel strains displaying higher infectivity [27,30] and mortality [28,29] rates. It is therefore expected that novel mutations in the antibody recognition site [47–49] or in the viral target of smart drugs under development [50] will arise when the selective pressure generated by the anti-viral treatments is applied to the general population. Hence, to avoid the problem of resistant clones and frailty in the immune system, our strategy shifted the focus of the therapy from targeting viral proteins towards the cellular receptor. This is also the molecular mechanism proposed for some active principles present in natural products [51–53]. In our study, the identification of the ACE2-K353 residue as a key determinant for the viral uptake on the target cell [12] provided the rational basis for a structure-function approach prompting us to design a masking strategy that could be independent from viral mutations.

It is worth pointing out that the mechanism of the viral interaction with the ACE2-K353 is fairly well conserved among different species of the *Orthocoronavirinae* subfamily, including SARS-CoV-2 and its variants. The reason for this conservation might be ascribed to the complex multistep molecular process for viral entry into the host cell, which cannot be easily modified by mutations. In fact, in order to infect the cell, the virus needs to go through several reactions, including: i) the S1 domain of S protein must be proteolytically digested by the S2 domain to unmask the residue E401 that interacts with ACE2, ii) the primed S1 can then bind to the K353 residue and iii) it is only afterwards that the S1 can create the breach needed to inject the viral RNA into the host cell [54]. Thus, it is unlikely that a single mutation could be sufficient to move the whole multistep mechanism onto another domain of the ACE2 or to another membrane protein of the target cell. In fact, none of the known variants modifies the ACE2 binding site, while single mutations in the SARS-CoV-2 S can change the viral affinity or specificity for the ACE2-K353 allowing a higher individual susceptibility and/or faster infectivity [55], or changing the amino acid specificity at the K353 recognizing histidine instead of lysin [49]. All these data point to the compulsory requirement for the viruses of the *Orthocoronavirinae* subfamily to use the 353 amino acid of ACE2, as the entry point for the cellular infection: therefore, our aptamers sterically masking the domain surrounding this residue can be considered as an efficient strategy to inhibit or hamper the susceptibility to the SARS-CoV-2 infection.

We can assume that targeting the ACE2 receptor might expose some people to side effects since ACE2 is a significant enzyme catalyzing and inactivating angiotensin II, a peptide hormone of the renin-angiotensin-aldosterone-system (RAAS) modulating several physiological and pathophysiological functions, including vasopressor activity, adrenergic tone, bradykinin release, blood volume, oxidative burst, the release of pro-inflammatory chemokines and cardiac and endothelium remodeling [56]. However, to the best of our knowledge, the viral site of interaction maps to a region of the molecule that is distinct from the enzymatic domain [57]. It is thus conceivable that the reversible binding of molecules at the region surrounding K353 might not influence the homeostatic activity of the enzyme. Moreover, for future clinical applications, the choice of short-strand oligonucleotides as macromolecules for the steric interference with S offer several advantages over other possible choices like antibodies or small peptides. For instance, nucleic acids have faster tissue uptake/penetration and limited half-life compared to antibodies, allowing a more efficient reverse control of the therapy. Furthermore, aptamers have almost no batch-to-batch variation and an immunogenicity that is inexistent or lower than peptides while conserving a similar high selectivity for the target, thus reducing the likelihood of major toxicity and unpredictable adverse reactions [58].

The potential therapeutic applications foreseen for the aptamers identified in our study span from prevention in subjects at high risk of infection to the cure of SARS-CoV-2 infection and its variants. Indeed, the prevention of viral cell-to cell spread, which generally involves the release of a large amount of new viral particles from the infected cell into the extracellular environment, would be helpful to significantly reduce the SARS-CoV-2 titer and to halt the virus spreading into the pulmonary/alveolar region of the lung and reaching distant vital organs such as the heart and brain. Indeed, simultaneous heart and brain damage contribute to the onset of severe COVID-19 leading to death [59]. Our aptamers will act to safely prevent heterogeneity in contagiousness and the occurrence of superspreading events among asymptomatic and

symptomatic infected individuals.

Therefore, thanks to the high target selectivity and affinity, the lack of immunogenicity and limited side effects, therapeutic aptamers we have identified could be a winning strategy, complementary to vaccines and monoclonal antibodies, for the rapid prevention and treatment of COVID-19, and to limit disease progression during undetected early infection. In addition, aptamers may be required to provide protection in those persons who might not have a robust protective response after vaccination. Further *in vivo* experiments to assess the therapeutic or prophylactic efficacy of aptamers would be a major advance in the control of the COVID-19 pandemic.

Funding

Grant no. 2020-1096 Fondazione Cariplo to P.C., Fondo straordinario of the University of Milan "Ricerche emergenza coronavirus" to P. C., Internal funds of Scuola Superiore Sant'Anna to V.L., Internal funds of Italian Institute of Technology to A.R.

CRediT authorship contribution statement

VL, PC, AR: Conceptualization. **EB, AV, CM, MR, GDV, MC:** Data collection. **PC:** Data analysis and interpretations. **PC:** Supervision. **PC, EB, LD, RDF, MR, CM, AV:** Methodology. **PC, RDF:** Resources. **PC, EB, AV:** Writing – original draft. **VL, PC, AR:** Critical revision of the manuscript.

Competing interest

The authors declare no competing interest.

Data availability

The data that support the findings of this study are available from the senior author (paolo.ciana@unimi.it) upon reasonable request.

Acknowledgments

The FP7 WeNMR (project# 261572), H2020 West-Life (project# 675858), the EOSC-hub (project# 777536) and the EGI-ACE (project# 101017567) European e-Infrastructure projects are acknowledged for the use of their web portals, which make use of the EGI infrastructure with the dedicated support of CESNET-MCC, INFN-PADOVA-STACK, INFN-LNL-2, NCG-INGRID-PT, TW-NCHC, CESGA, IFCA-LCG2, UA-BITP, SURFsara and NIKHEF, and the additional support of the national GRID Initiatives of Belgium, France, Italy, Germany, the Netherlands, Poland, Portugal, Spain, UK, Taiwan and the US Open Science Grid.

Appendix A. Supporting information

Supplementary data associated with this article can be found in the online version at doi:10.1016/j.phrs.2021.105982.

References

[1] C. Robba, D. Battaglini, P. Pelosi, P.R.M. Rocco, Multiple organ dysfunction in SARS-CoV-2: MODS-CoV-2, Expert Rev. Respir. Med. 14 (9) (2020) 865–868.
[2] P. Cappy, D. Candotti, V. Sauvage, Q. Lucas, L. Boizeau, J. Gomez, V. Enouf, L. Chabli, J. Pillonel, P. Tiberghien, No evidence of SARS-CoV-2 transfusion transmission despite RNA detection in blood donors showing symptoms after donation, Blood 136 (16) (2020) 1888–1891.
[3] R. Wölfel, V.M. Corman, W. Guggemos, M. Seilmaier, S. Zange, M.A. Müller, D. Niemeyer, T.C. Jones, P. Vollmar, C. Rothe, Virological assessment of hospitalized patients with COVID-2019, Nature 581 (7809) (2020) 465–469.
[4] M.I. Andersson, C.V. Arancibia-Carcamo, K. Auckland, J.K. Baillie, E. Barnes, T. Beneke, S. Bibi, T. Brooks, M. Carroll, D. Crook, SARS-CoV-2 RNA detected in blood products from patients with COVID-19 is not associated with infectious virus, Wellcome Open Res. 5 (2020).
[5] F. Moccia, A. Gerbino, V. Lionetti, M. Miragoli, L.M. Munaron, P. Pagliaro, T. Pasqua, C. Penna, C. Rocca, M. Samaja, T. Angelone, COVID-19-associated cardiovascular morbidity in older adults: a position paper from the Italian society of cardiovascular researches, Geroscience 42 (4) (2020) 1021–1049.
[6] I. Razeghian-Jahromi, M.J. Zibaeenezhad, Z. Lu, E. Zahra, R. Mahboobeh, V. Lionetti, Angiotensin-converting enzyme 2: a double-edged sword in COVID-19 patients with an increased risk of heart failure, Heart Fail Rev. 26 (2) (2021) 371–380.
[7] J. Lan, J. Ge, J. Yu, S. Shan, H. Zhou, S. Fan, Q. Zhang, X. Shi, Q. Wang, L. Zhang, X. Wang, Structure of the SARS-CoV-2 spike receptor-binding domain bound to the ACE2 receptor, Nature 581 (7807) (2020) 215–220.
[8] R. Yan, Y. Zhang, Y. Li, L. Xia, Y. Guo, Q. Zhou, Structural basis for the recognition of SARS-CoV-2 by full-length human ACE2, Science 367 (6485) (2020) 1444–1448.
[9] H. Zhang, J.M. Penninger, Y. Li, N. Zhong, A.S. Slutsky, Angiotensin-converting enzyme 2 (ACE2) as a SARS-CoV-2 receptor: molecular mechanisms and potential therapeutic target, Intensive Care Med. 46 (4) (2020) 586–590.
[10] J. Shang, G. Ye, K. Shi, Y. Wan, C. Luo, H. Aihara, Q. Geng, A. Auerbach, F. Li, Structural basis of receptor recognition by SARS-CoV-2, Nature 581 (7807) (2020) 221–224.
[11] F. Li, W. Li, M. Farzan, S.C. Harrison, Structure of SARS coronavirus spike receptor-binding domain complexed with receptor, Science 309 (5742) (2005) 1864–1868.
[12] X. Zhao, D. Chen, R. Szabla, M. Zheng, G. Li, P. Du, S. Zheng, X. Li, C. Song, R. Li, J. T. Guo, M. Junop, H. Zeng, H. Lin, Broad and differential animal angiotensin-converting enzyme 2 receptor usage by SARS-CoV-2, J. Virol. 94 (18) (2020).
[13] J. Stebbing, A. Phelan, I. Griffin, C. Tucker, O. Oechsle, D. Smith, P. Richardson, COVID-19: combining antiviral and anti-inflammatory treatments, Lancet Infect. Dis. 20 (4) (2020) 400–402.
[14] W.H.O. Solidarity Trial Consortium, H. Pan, R. Peto, A.M. Henao-Restrepo, M. P. Preziosi, V. Sathiyamoorthy, Q. Abdool Karim, M.M. Alejandria, C. Hernandez Garcia, M.P. Kieny, R. Malekzadeh, S. Murthy, K.S. Reddy, M. Roses Periago, P. Abi Hanna, F. Ader, A.M. Al-Bader, A. Alhasawi, E. Allum, A. Alotaibi, C.A. Alvarez-Moreno, S. Appadoo, A. Asiri, P. Aukrust, A. Barratt-Due, S. Bellani, M. Branca, H. B.C. Cappel-Porter, N. Cerrato, T.S. Chow, N. Como, J. Eustace, P.J. Garcia, S. Godbole, E. Gotuzzo, L. Griskevicius, R. Hamra, M. Hassan, M. Hassany, D. Hutton, I. Irmansyah, L. Jancoriene, J. Kirwan, S. Kumar, P. Lennon, G. Lopardo, P. Lydon, N. Magrini, T. Maguire, S. Manevska, O. Manuel, S. McGinty, M. T. Medina, M.L. Mesa Rubio, M.C. Miranda-Montoya, J. Nel, E.P. Nunes, M. Perola, A. Portoles, M.R. Rasmin, A. Raza, H. Rees, P.P.S. Reges, C.A. Rogers, K. Salami, M. I. Salvadori, N. Sinani, J.A.C. Sterne, M. Stevanovikj, E. Tacconelli, K.A. O. Tikkinen, S. Trelle, H. Zaid, J.A. Rottingen, S. Swaminathan, Repurposed antiviral drugs for covid-19 - interim WHO solidarity trial results, N. Engl. J. Med. 384 (6) (2021) 497–511.
[15] P. Recovery Collaborative Group, W.S. Horby, J.R. Lim, M. Emberson, J. L. Mafham, L. Bell, N. Linsell, C. Staplin, A. Brightling, E. Ustianowski, B. Elmahi, C. Prudon, T. Green, D. Felton, K. Chadwick, C. Rege, L.C. Fegan, S.N. Chappell, T. Faust, K. Jaki, A. Jeffery, K. Montgomery, E. Rowan, J.K. Juszczak, R. Baillie, M. J.Landray Haynes, Dexamethasone in hospitalized patients with covid-19, N. Engl. J. Med. 384 (8) (2021) 693–704.
[16] N. Ben-Zuk, I.-D. Dechtman, I. Henn, L. Weiss, A. Afriat, E. Krasner, Y. Gal, Potential prophylactic treatments for COVID-19, Viruses 13 (7) (2021) 1292.
[17] L. Runfeng, H. Yunlong, H. Jicheng, P. Weiqi, M. Qinhai, S. Yongxia, L. Chufang, Z. Jin, J. Zhenhua, J. Haiming, Z. Kui, H. Shuxiang, D. Jun, L. Xiaobo, H. Xiaotao, W. Lin, Z. Nanshan, Y. Zifeng, Lianhuaqingwen exerts anti-viral and anti-inflammatory activity against novel coronavirus (SARS-CoV-2), Pharm. Res. 156 (2020), 104761.
[18] E.L. Leung, H.D. Pan, Y.F. Huang, X.X. Fan, W.Y. Wang, F. He, J. Cai, H. Zhou, L. Liu, The scientific foundation of chinese herbal medicine against COVID-19, Engineering 6 (10) (2020) 1099–1107.
[19] N. Shi, B. Liu, N. Liang, Y. Ma, Y. Ge, H. Yi, H. Wo, H. Gu, Y. Kuang, S. Tang, Y. Zhao, L. Tong, S. Liu, C. Zhao, R. Chen, W. Bai, Y. Fan, Z. Shi, L. Li, J. Liu, H. Gu, Y. Zhi, Z. Wang, Y. Li, H. Li, J. Wang, L. Jiao, Y. Tian, Y. Xiong, R. Huo, X. Zhang, J. Bai, H. Chen, L. Chen, Q. Feng, T. Guo, Y. Hou, G. Hu, X. Hu, Y. Hu, J. Huang, Q. Huang, S. Huang, L. Ji, H. Jin, X. Lei, C. Li, G. Wu, J. Li, M. Li, Q. Li, X. Li, H. Liu, J. Liu, Z. Liu, Y. Ma, Y. Mao, L. Mo, H. Na, J. Wang, F. Song, S. Sun, D. Wang, M. Wang, X. Wang, Y. Wang, Y. Wang, W. Wu, L. Wu, Y. Xiao, H. Xie, H. Xu, S. Xu, R. Xue, C. Yang, K. Yang, P. Yang, S. Yuan, G. Zhang, J. Zhang, L. Zhang, S. Zhao, W. Zhao, K. Zheng, Y. Zhou, J. Zhu, T. Zhu, G. Li, W. Wang, H. Zhang, Y. Wang, Y. Wang, Association between early treatment with Qingfei Paidu decoction and favorable clinical outcomes in patients with COVID-19: a retrospective multicenter cohort study, Pharm. Res. 161 (2020), 105290.
[20] G. Forni, A. Mantovani, C.-C.A.N. Lin, COVID-19 vaccines: where we stand and challenges ahead, Cell Death Differ. 28 (2) (2021) 626–639.
[21] N. Suryadevara, S. Shrihari, P. Gilchuk, L.A. VanBlargan, E. Binshtein, S.J. Zost, R. S. Nargi, R.E. Sutton, E.S. Winkler, E.C. Chen, M.E. Fouch, E. Davidson, B. J. Doranz, R.E. Chen, P.Y. Shi, R.H. Carnahan, L.B. Thackray, M.S. Diamond, J. E. Crowe Jr., Neutralizing and protective human monoclonal antibodies recognizing the N-terminal domain of the SARS-CoV-2 spike protein, Cell 184 (9) (2021), 2316-2331 e15.
[22] E. Andreano, E. Nicastri, I. Paciello, P. Pileri, N. Manganaro, G. Piccini, A. Manenti, E. Pantano, A. Kabanova, M. Troisi, F. Vacca, D. Cardamone, C. De Santi, J. L. Torres, G. Ozorowski, L. Benincasa, H. Jang, C. Di Genova, L. Depau, J. Brunetti, C. Agrati, M.R. Capobianchi, C. Castilletti, A. Emiliozzi, M. Fabbiani, F. Montagnani, L. Bracci, G. Sautto, T.M. Ross, E. Montomoli, N. Temperton, A. B. Ward, C. Sala, G. Ippolito, R. Rappuoli, Extremely potent human monoclonal antibodies from COVID-19 convalescent patients, Cell 184 (7) (2021), 1821-1835 e16.

[23] J. Fernandez, J. Gratacos-Gines, P. Olivas, M. Costa, S. Nieto, D. Mateo, M. B. Sanchez, F. Aguilar, O. Bassegoda, P. Ruiz, B. Caballol, A. Pocurull, J. Llach, M. J. Mustieles, J. Cid, E. Reverter, N.D. Toapanta, M. Hernandez-Tejero, J. A. Martinez, J. Claria, C. Fernandez, J. Mensa, V. Arroyo, P. Castro, M. Lozano, G. Covid, Clinic critical care, plasma exchange: an effective rescue therapy in critically Ill patients with coronavirus disease 2019 infection, Crit. Care Med. 48 (12) (2020) e1350–e1355.

[24] J. Madhusoodanan, Inner workings: advances in infectious disease treatment promise to expand the pool of donor organs, Proc. Natl. Acad. Sci. USA 118 (8) (2021).

[25] T.M. Cook, J.V. Roberts, Impact of vaccination by priority group on UK deaths, hospital admissions and intensive care admissions from COVID-19, Anaesthesia 76 (5) (2021) 608–616.

[26] A. Casadevall, J.P. Henderson, M.J. Joyner, L.A. Pirofski, SARS-CoV-2 variants and convalescent plasma: reality, fallacies, and opportunities, J. Clin. Invest 131 (7) (2021).

[27] N.G. Davies, S. Abbott, R.C. Barnard, C.I. Jarvis, A.J. Kucharski, J.D. Munday, C.A. B. Pearson, T.W. Russell, D.C. Tully, A.D. Washburne, T. Wenseleers, A. Gimma, W. Waites, K.L.M. Wong, K. van Zandvoort, J.D. Silverman, C.C.-W. Group, C.-G. U. Consortium, K. Diaz-Ordaz, R. Keogh, R.M. Eggo, S. Funk, M. Jit, K.E. Atkins, W. J. Edmunds, Estimated transmissibility and impact of SARS-CoV-2 lineage B.1.1.7 in England, Science 372 (6538) (2021).

[28] J. Hu, C. Li, S. Wang, T. Li, H. Zhang, Genetic variants are identified to increase risk of COVID-19 related mortality from UK Biobank data, medRxiv (2020).

[29] R. Challen, E. Brooks-Pollock, J.M. Read, L. Dyson, K. Tsaneva-Atanasova, L. Danon, Risk of mortality in patients infected with SARS-CoV-2 variant of concern 202012/1: matched cohort study, BMJ 372 (2021) n579.

[30] A. Khan, T. Zia, M. Suleman, T. Khan, S.S. Ali, A.A. Abbasi, A. Mohammad, D. Q. Wei, Higher infectivity of the SARS-CoV-2 new variants is associated with K417N/T, E484K, and N501Y mutants: an insight from structural data, J. Cell Physiol. (2021).

[31] P. Dorr, M. Westby, S. Dobbs, P. Griffin, B. Irvine, M. Macartney, J. Mori, G. Rickett, C. Smith-Burchnell, C. Napier, R. Webster, D. Armour, D. Price, B. Stammen, A. Wood, M. Perros, Maraviroc (UK-427,857), a potent, orally bioavailable, and selective small-molecule inhibitor of chemokine receptor CCR5 with broad-spectrum anti-human immunodeficiency virus type 1 activity, Antimicrob. Agents Chemother. 49 (11) (2005) 4721–4732.

[32] C. Tuerk, L. Gold, Systematic evolution of ligands by exponential enrichment: RNA ligands to bacteriophage T4 DNA polymerase, Science 249 (4968) (1990) 505–510.

[33] A.D. Keefe, S.T. Cload, SELEX with modified nucleotides, Curr. Opin. Chem. Biol. 12 (4) (2008) 448–456.

[34] J. Liu, B. Guo, RNA-based therapeutics for colorectal cancer: updates and future directions, Pharm. Res. 152 (2020), 104550.

[35] Y. Shen, J. Maupetit, P. Derreumaux, P. Tuffery, Improved PEP-FOLD approach for peptide and miniprotein structure prediction, J. Chem. Theory Comput. 10 (10) (2014) 4745–4758.

[36] A. Conforti, E. Marra, F. Palombo, G. Roscilli, M. Rava, V. Fumagalli, A. Muzi, M. Maffei, L. Luberto, L. Lione, COVID-eVax, an electroporated plasmid DNA vaccine candidate encoding the SARS-CoV-2 Receptor Binding Domain, elicits protective immune responses in animal models of COVID-19, bioRxiv (2021).

[37] M. Zuker, Mfold web server for nucleic acid folding and hybridization prediction, Nucleic Acids Res. 31 (13) (2003) 3406–3415.

[38] M. van Dijk, A.M. Bonvin, 3D-DART: a DNA structure modelling server (Web Server issue), Nucleic Acids Res. 37 (2009) W235–W239.

[39] Z. Zhuo, Y. Yu, M. Wang, J. Li, Z. Zhang, J. Liu, X. Wu, A. Lu, G. Zhang, B. Zhang, Recent advances in SELEX technology and aptamer applications in biomedicine, Int J. Mol. Sci. 18 (10) (2017).

[40] M. Sorokina, M.C.T. J, S. Barrera-Vilarmau, R. Paschke, I. Papasotiriou, J. Rodrigues, P.L. Kastritis, Structural models of human ACE2 variants with SARS-CoV-2 spike protein for structure-based drug design, Sci. Data 7 (1) (2020) 309.

[41] G.C.P. van Zundert, J. Rodrigues, M. Trellet, C. Schmitz, P.L. Kastritis, E. Karaca, A. S.J. Melquiond, M. van Dijk, S.J. de Vries, A. Bonvin, The HADDOCK2.2 web server: user-friendly integrative modeling of biomolecular complexes, J. Mol. Biol. 428 (4) (2016) 720–725.

[42] M.N. Maas, J.C.J. Hintzen, P.M.G. Loffler, J. Mecinovic, Targeting SARS-CoV-2 spike protein by stapled hACE2 peptides, Chem. Commun. 57 (26) (2021) 3283–3286.

[43] C. Kim, D.K. Ryu, J. Lee, Y.I. Kim, J.M. Seo, Y.G. Kim, J.H. Jeong, M. Kim, J.I. Kim, P. Kim, J.S. Bae, E.Y. Shim, M.S. Lee, M.S. Kim, H. Noh, G.S. Park, J.S. Park, D. Son, Y. An, J.N. Lee, K.S. Kwon, J.Y. Lee, H. Lee, J.S. Yang, K.C. Kim, S.S. Kim, H. M. Woo, J.W. Kim, M.S. Park, K.M. Yu, S.M. Kim, E.H. Kim, S.J. Park, S.T. Jeong, C. H. Yu, Y. Song, S.H. Gu, H. Oh, B.S. Koo, J.J. Hong, C.M. Ryu, W.B. Park, M.D. Oh, Y.K. Choi, S.Y. Lee, A therapeutic neutralizing antibody targeting receptor binding domain of SARS-CoV-2 spike protein, Nat. Commun. 12 (1) (2021) 288.

[44] Y. Song, J. Song, X. Wei, M. Huang, M. Sun, L. Zhu, B. Lin, H. Shen, Z. Zhu, C. Yang, Discovery of aptamers targeting the receptor-binding domain of the SARS-CoV-2 spike glycoprotein, Anal. Chem. 92 (14) (2020) 9895–9900.

[45] J. Verma, N. Subbarao, A comparative study of human betacoronavirus spike proteins: structure, function and therapeutics, Arch. Virol. 166 (3) (2021) 697–714.

[46] D. Planas, T. Bruel, L. Grzelak, F. Guivel-Benhassine, I. Staropoli, F. Porrot, C. Planchais, J. Buchrieser, M.M. Rajah, E. Bishop, M. Albert, F. Donati, M. Prot, S. Behillil, V. Enouf, M. Maquart, M. Smati-Lafarge, E. Varon, F. Schortgen, L. Yahyaoui, M. Gonzalez, J. De Seze, H. Pere, D. Veyer, A. Seve, E. Simon-Loriere, S. Fafi-Kremer, K. Stefic, H. Mouquet, L. Hocqueloux, S. van der Werf, T. Prazuck, O. Schwartz, Sensitivity of infectious SARS-CoV-2 B.1.1.7 and B.1.351 variants to neutralizing antibodies, Nat. Med. 27 (5) (2021) 917–924.

[47] R.E. Chen, X. Zhang, J.B. Case, E.S. Winkler, Y. Liu, L.A. VanBlargan, J. Liu, J. M. Errico, X. Xie, N. Suryadevara, P. Gilchuk, S.J. Zost, S. Tahan, L. Droit, J. S. Turner, W. Kim, A.J. Schmitz, M. Thapa, D. Wang, A.C.M. Boon, R.M. Presti, J. A. O'Halloran, A.H.J. Kim, P. Deepak, D. Pinto, D.H. Fremont, J.E. Crowe Jr., D. Corti, H.W. Virgin, A.H. Ellebedy, P.Y. Shi, M.S. Diamond, Resistance of SARS-CoV-2 variants to neutralization by monoclonal and serum-derived polyclonal antibodies, Nat. Med. 27 (4) (2021) 717–726.

[48] P. Wang, M.S. Nair, L. Liu, S. Iketani, Y. Luo, Y. Guo, M. Wang, J. Yu, B. Zhang, P. D. Kwong, B.S. Graham, J.R. Mascola, J.Y. Chang, M.T. Yin, M. Sobieszczyk, C. A. Kyratsous, L. Shapiro, Z. Sheng, Y. Huang, D.D. Ho, Antibody resistance of SARS-CoV-2 variants B.1.351 and B.1.1.7, Nature 593 (7857) (2021) 130–135.

[49] Y. Liu, J. Liu, K.S. Plante, J.A. Plante, X. Xie, X. Zhang, Z. Ku, Z. An, D. Scharton, C. Schindewolf, V.D. Menachery, P.Y. Shi, S.C. Weaver, The N501Y spike substitution enhances SARS-CoV-2 transmission, bioRxiv (2021) 2021.03.08.434499.

[50] J.R. Mascola, B.S. Graham, A.S. Fauci, SARS-CoV-2 viral variants-tackling a moving target, JAMA 325 (13) (2021) 1261–1262.

[51] H. Wu, J. Wang, Y. Yang, T. Li, Y. Cao, Y. Qu, Y. Jin, C. Zhang, Y. Sun, Preliminary exploration of the mechanism of Qingfei Paidu decoction against novel coronavirus pneumonia based on network pharmacology and molecular docking technology, Acta Pharm. Sin. 55 (3) (2020) 374–383.

[52] Y.-F. Huang, C. Bai, F. He, Y. Xie, H. Zhou, Review on the potential action mechanisms of Chinese medicines in treating Coronavirus Disease 2019 (COVID-19), Pharmacol. Res. 158 (2020), 104939.

[53] D. Xu, Y. Xu, Z. Wang, Mechanism of Qingfeipaidu decoction on COVID-19 based on network pharmacology, Pharm. Clin. Chin. Mater. Med. (2020) 2020.

[54] J. Yang, S.J.L. Petitjean, M. Koehler, Q. Zhang, A.C. Dumitru, W. Chen, S. Derclaye, S.P. Vincent, P. Soumillion, D. Alsteens, Molecular interaction and inhibition of SARS-CoV-2 binding to the ACE2 receptor, Nat. Commun. 11 (1) (2020) 4541.

[55] S.S. Abdool Karim, T. de Oliveira, New SARS-CoV-2 variants - clinical, public health, and vaccine implications, N. Engl. J. Med. 384 (19) (2021) 1866–1868.

[56] O. Wiese, A.E. Zemlin, T.S. Pillay, Molecules in pathogenesis: angiotensin converting enzyme 2 (ACE2), J. Clin. Pathol. 74 (5) (2021) 285–290.

[57] P. Towler, B. Staker, S.G. Prasad, S. Menon, J. Tang, T. Parsons, D. Ryan, M. Fisher, D. Williams, N.A. Dales, M.A. Patane, M.W. Pantoliano, ACE2 X-ray structures reveal a large hinge-bending motion important for inhibitor binding and catalysis, J. Biol. Chem. 279 (17) (2004) 17996–18007.

[58] J. Zhou, J. Rossi, Aptamers as targeted therapeutics: current potential and challenges, Nat. Rev. Drug Disco 16 (3) (2017) 181–202.

[59] V. Lionetti, S. Bollini, R. Coppini, A. Gerbino, A. Ghigo, G. Iaccarino, R. Madonna, F. Mangiacapra, M. Miragoli, F. Moccia, L. Munaron, P. Pagliaro, A. Parenti, T. Pasqua, C. Penna, F. Quaini, C. Rocca, M. Samaja, L. Sartiani, T. Soda, C. G. Tocchetti, T. Angelone, Understanding the heart-brain axis response in COVID-19 patients: a suggestive perspective for therapeutic development, Pharm. Res. 168 (2021), 105581.